applied sciences

MDPI

Article

Characteristics of Perimeter Rock Damage in a Bottom-Pumping Roadway under the Influence of Mining Activities and Rational Location Studies: A Case Study

Libin Bai [1,2], Fengfeng Wu [1,*], Peiju Yang [1], Shurong Zhang [1] and Bin Li [1]

[1] School of Mines, China University of Mining and Technology, Xuzhou 221000, China
[2] Liuta Coal Mine, China National Energy Shendong Coal Group, Ordos 221000, China
* Correspondence: wufengfeng@cumt.edu.cn

Abstract: With the aim of determining the damage characteristics and a reasonable positional arrangement of the surrounding rock in a bottom-pumping roadway influenced by mining in a high-gas mine, the boundary equation for the plastic zone of the surrounding rock in a circular roadway under an unequal compressive stress field was adopted to analyze the relationship between the distribution characteristics of the plastic zone of the bottom-pumping roadway and the stability of the rock surrounding the bottom-pumping roadway under different bidirectional stress ratios. This was carried out in the bottom-pumping roadway of the working face of Licun coal mine 3301 as the engineering background, where the nature of the coal seams mined is bituminous coal, and the absolute gas outflow is 0.5 m^3/min^{-1}. A numerical simulation was used to analyze the distribution characteristics of the surrounding rock stress and the bidirectional stress ratio, as well as the deformation and damage characteristics of the surrounding rock at different positions in the bottom-pumping roadway. A numerical simulation was applied to analyze the distribution characteristics of the surrounding rock stress and the two-way stress ratio, as well as the deformation and damage characteristics of the rock surrounding the bottom-pumping roadway when the bottom-pumping roadway was arranged in different locations. The results show that, with an increase in the bidirectional stress ratio, the plastic zone of the perimeter rock in the bottom-pumping roadway shows nonuniform "butterfly" distribution characteristics, which seriously affects the stability of the rock on the perimeter of the roadway; the stress on the bottom plate of the working face after excavation can be divided into four areas according to the size of the bidirectional stress ratio and the stress loading and unloading states. In addition, the size of the perimeter rock deformation can be sorted into four areas according to the damage range of the perimeter of the rock plastic zone in the bottom-pumping roadway. The size of the deformation in the surrounding rock can be sorted as follows: unpressurized high-stress ratio > unpressurized stress ratio stable area > pressurized low-stress ratio area > original rock stress ratio area. Accordingly, we found that the reasonable location of the bottom-pumping roadway is arranged at the 15 m position outside the hollow area below the coal pillar, along the limestone upper medium-grained sandstone layer along the bottom. The study's results were applied to the field. The industrial experiments on the site show that the deformation of the surrounding rock is reasonable when the bottom-pumping roadway is dug along the limestone roof and arranged 15 m outside the fault of the mining hollow area below the coal pillar.

Keywords: bidirectional stress ratio; bottom-pumping alley; reasonable location; surrounding rock deformation damage characteristics

Citation: Bai, L.; Wu, F.; Yang, P.; Zhang, S.; Li, B. Characteristics of Perimeter Rock Damage in a Bottom-Pumping Roadway under the Influence of Mining Activities and Rational Location Studies: A Case Study. *Appl. Sci.* **2024**, *14*, 2727. https://doi.org/10.3390/app14072727

Academic Editor: Stefano Invernizzi

Received: 23 February 2024
Revised: 14 March 2024
Accepted: 14 March 2024
Published: 25 March 2024

1. Introduction

With the gradual expansion of deep mining for coal resources in China, coal and gas outbursts in mines have become more and more serious. To ensure safe production in mines, it is extremely important to arrange the bottom pumping roadway on the floor of the working face for gas drainage from the upper working face [1–5]. However, when the working face is being mined back, the bottom plate is affected by the mining of the working face, and the stress is transferred to the deep part of the bottom plate of the working face of the roadway, which redistributes the stress in the rock surrounding the bottom plate. Then, there is a nonuniform stress field, i.e., a two-way unequal compressive stress field, in the rock surrounding the bottom plate, which results in different degrees of damage to the rock surrounding the bottom plate in different locations [6–8]. The damage to the bottom plate rock at different locations is caused by the nonuniform stress field. Therefore, obtaining the distribution law and damage characteristics of the two-way unequal compressive stress field in the base plate rock under the influence of mining in the working face is the key factor in determining the reasonable location of the bottom-pumping tunnel.

Experts and scholars at home and abroad have conducted much research concerning the distribution law and damage characteristics of two-way unequal compressive stress fields in the rock surrounding the base plate under the influence of mining in the working face and have achieved remarkable results. Among them are Li Yong'en et al. [9–12]. Given the contradiction between the bottom-pumping lane and the pressurized water, they established a boundary equation for the plastic zone of the circular lane under a two-way unequal compressive stress field, analyzed the damage characteristics of the plastic zone of the surrounding rock in the bottom-pumping lane with the different values of the two-way stress ratio, and determined the reasonable location of the bottom-pumping lane according to the damage characteristics of the plastic zone. Li Ang et al. [13–15] applied a research method combining theoretical analysis and numerical simulation to analyze the stress distribution characteristics of the bottom plate of the working face under the influence of mining and the damage evolution characteristics of the surrounding rock in the plastic zone. They also obtained the distribution law of the supporting pressure of the rock layer of the bottom plate and the damage range of the rock layer in the bottom plate under the influence of mining. Wang et al. [16–19] created a tangential stress equation for the surrounding rock in a two-way unequal pressure stress field of a circular roadway, which was derived using the method of angle-preserving transformation in the complex function, and the formula for calculating the plastic zone of the circular roadway under the condition of two-way unequal pressure was further obtained based on the Moore–Coulomb strength criterion. Zhu Ye et al. [20–22] investigated the stability of the base plate under different stress field environments through theoretical analysis and numerical calculation and pointed out that the stresses in the base plate peripheral rock under the influence of mining were significantly different from each other, and the variability of the stress environments was the main reason for the variability in the stresses in the base plate's peripheral rock. By establishing a physical similarity model, Gao Shigang et al. explored the reasonable arrangement of mining roadways in middle and lower coal seams in close-distance coal seam mining [23]. Through numerical calculations, Chi Xiaolou et al. [24,25] analyzed the distribution law of stress fields and the evolution characteristics of the plastic zone of a rock mining face's bottom plate with a change in the advancing degree. They concluded that, in the process of the advancing face, the rock at the periphery of the bottom plate appeared to be the supporting stress zone, and with the forward advancement of the working face, there were differences in the stress zone supporting the bottom, and the plastic zone of the bottom plate peripheral rock is different from the different supporting stress zone. In addition, many scholars [26,27] have researched the stress environment of the peripheral rock of the floor roadway and the damage characteristics of the peripheral rock. They proposed using the theory of elastic mechanics to deduce the stress distribution law of the peripheral rock of the floor, and they combined it with the relevant damage criterion to calculate the maximum depth of destruction of the floor. Some scholars have also analyzed the layer relationship between the floor roadway of the working face and the coal pillar above it, as well as the quarry, by collecting on-site data [28,29]. The damage mechanism of the bottom roadway under the influence of mining and the deformation of the roadway's peripheral rock are also analyzed in depth. However, the peripheral rock of the bottom roadway under the influence of mining is in the nonuniform stress area, and the peripheral rock of the bottom roadway is affected by the two-way unequal compressive stress [30]. In the past, most scholars have focused on the change in support pressure when they studied the damage characteristics of the bottom plate and neglected the influence of a two-way unequal compressive stress field on damage to the bottom plate roadway. In recent years, a few scholars have deduced the boundary equation of the surrounding rock plastic zone under a two-way unequal compressive stress field and more comprehensively analyzed the damage characteristics of the surrounding rock plastic zone of a subgrade roadway under a nonuniform stress field, which put forward a novel idea for analyzing the damage characteristics of the surrounding rock plastic zone of a subgrade roadway under nonuniform stress fields.

To summarize, different two-way unequal compressive stress fields in the base plate under the influence of mining are the main reason for the differences in the damage characteristics of the plastic zone of the surrounding rock in the base plate roadway. There is currently less research on the distribution law of two-way unequal compressive stress fields in the base plate and the damage characteristics of the plastic zone of the surrounding rock in the base plate under two-way unequal compressive stress fields. The authors take the bottom-pumping roadway of the working face of Licun coal mine 3301 as the engineering background, use theoretical analysis to analyze the damage characteristics of the plastic zone of the surrounding rock under different bidirectional stress ratios in the bottom plate, and apply FLAC^{3D} 5.0 numerical simulation software. This is carried out to analyze the distribution law of the stress in the surrounding rock of the bottom plate and the characteristics of the distribution of bidirectional stress ratios. Furthermore, on the basis of the above, research is performed on the damage characteristics of the plastic zone of the bottom-pumping roadway when it is in different positions in the bottom plate, and then the reasonable position of the bottom-pumping roadway in the Licun coal mine is determined. The reasonable location of the bottom-pumping tunnel in the coal mine is determined, and the research results are used in the field to provide a reference basis for mines with the same geological conditions.

2. Research Background

2.1. Engineering Background

In the past, the Licun coal mine has had difficulty with gas extraction and drilling operations, along with low extraction efficiency. To ensure that the mine can meet the production requirements for the regionalization management of coal seam gas, there is an urgent need for the efficient extraction of coal seam gas in the bottom layout of the gas extraction roadway of the No. 3 coal. The working face of 3301 is mainly for mining No. 3 coal, the depth of the coal seam is about 540 m, and the average thickness of the coal is about 6 m. The No. 3 seam is stable and simple in structure, with a thickness variation coefficient of 0.24 and a recoverability coefficient of 100%, making it a stable and regionally recoverable coal seam. The average gas content is 14.52 m^3/t. The nature of the coal seam is bituminous coal, and the absolute gas outflow is 0.5 m^3/min^{-1}, which makes it a high-gas mine. The length of the working face is designed to be 160 m, and between the two working faces, there is a 30 m protective coal pillar. The roof is mainly composed of dark gray mudstone and sandy mudstone. The design length of the working face is 160 m, and there is a 30 m protection pillar between the two working faces. The whole caving method is used to deal with the goaf in the working face. According to the survey results, it can be seen that the No. 3 coal seam is a stable and simple structure within the whole mining coal seam, and the average dip angle of the coal seam is 10°. Its top plate is mainly dominated by dark gray mudstone, sandy mudstone, and siltstone, and the bottom plate is mainly black mudstone, sandy mudstone, and dark gray siltstone. Its working face schematic and the drilling column diagram of the top and bottom rock layers are shown in Figure 1. The plane diagram of the working face layout of 3301 is shown in Figure 2.

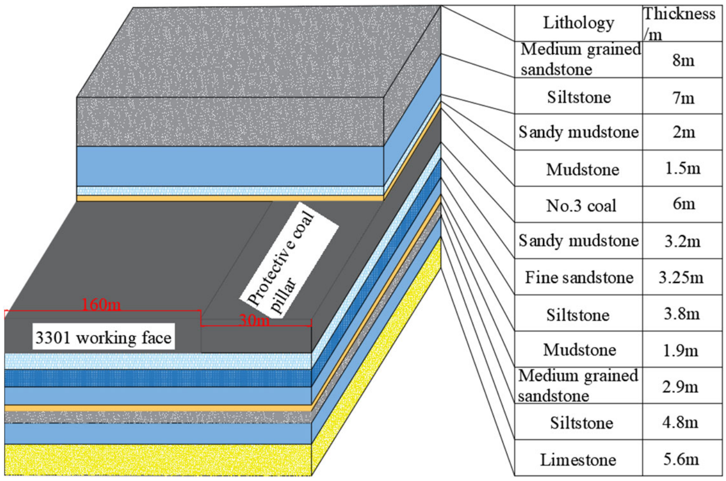

Figure 1. Schematic of 3301's working face and a column diagram of drill holes in the top and bottom rock strata.

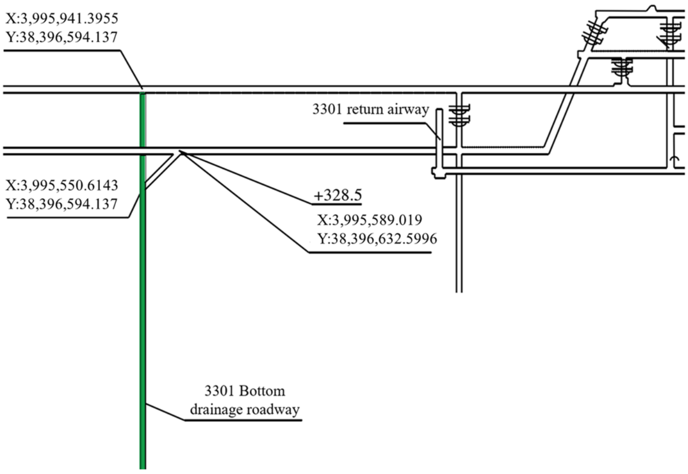

Figure 2. Plane diagram of the working face layout of 3301.

The process of roadway excavation may be affected by the SX anticline and its secondary structure. Within the scope of this influence, the lithology of the roadway side may change. The structure in the area is relatively simple, consisting of mainly wide and gentle folds. The direct water-filled aquifer of No. 3 coal is the roof sandstone fissure aquifer, and the unit water inflow of the borehole is the weak water content of the aquifer.

2.2. Determination of Mechanical Parameters of Surrounding Rock

To analyze the distribution of the bidirectionally unequal compressive stress field in the base plate of the working face and the damage characteristics of the plastic zone of the base plate's surrounding rock, samples of a coal rock body were collected from the top and bottom plates of the working face of 3301 where there was no obvious tectonic zone. Furthermore, the rock samples were processed into standard specimens, as shown in Figure 3 below, and the specimens were tested to determine the surrounding rock's physical and mechanical properties. The specimen size for the uniaxial compression test was h × φ = 100 mm × 50 mm, the specimen size for the Brazilian splitting test was h × φ = 25 mm × 50 mm, and the test specimen for the shear strength test was a 50 mm × 50 mm cube. Three specimens were tested in each group, and the test results were averaged. The displacement loading mode was used in the test, and the loading rate was 0.2 mm/min.

Figure 3. Coal rock body mechanical properties are part of the standard rock sample test damage map.

The test results were obtained by testing the physical and mechanical properties of the surrounding rock at the top and bottom of 3301's working face, as shown in Table 1 below.

Table 1. Statistical table of the results of the mechanical experiment on the coal rock body.

Lithology	Density ($kg \cdot m^{-3}$)	Elastic Modulus (GPa)	Normal Strength (GPa/m)	Tangential Strength (GPa/m)	Cohesive Force (MPa)	Internal Friction Angle (°)	Tensile Strength (MPa)
No. 3 Coal	1400	2.6	112	44.8	1.25	20	0.64
Mudstone	2510	5.4	228	91	9.34	27	1.99
No. 4 Coal	1400	2.7	113	45.1	1.2	19	0.59
Siltstone	2550	9.7	351.2	140	7.1	31	2.15
Calcareous Limestone	2800	10.4	464.4	185.7	16.08	36	8.05

3. Characteristics of Damage in the Plastic Zone of the Rock Surrounding the Base Plate under the Influence of Mining

When the working face is mined, the stress on the surrounding rock of the rock layer around the working face is transferred to the bottom plate due to mining. As a result, the stress field of the surrounding rock of the bottom plate is changed, and a nonuniform stress field is generated at different locations of the bottom plate. This results in different degrees of damage to the bottom plate of the working face at different locations. Furthermore, because of different positional relationships between the bottom-pumping roadway and the working face above it, the peripheral rock of the bottom-pumping roadway will inevitably be damaged to a different extent. Therefore, analyzing the damage characteristics of the peripheral rock of the bottom-pumping roadway under the influence of mining in the working face is crucial to determine the reasonable positional relationship between the bottom-pumping roadway and the working face.

3.1. Mechanical Mechanism of the Formation of the Plastic Zone in the Rock Surrounding the Floor Gas Drainage Roadway

From the theory of elastic mechanics, when the roadway is buried more than or equal to 20 times the radius of the roadway, the self-weight of the rock within the influence of the roadway can be ignored. Then, the original horizontal and vertical rock stress around the roadway can be simplified as a homogeneous load. Therefore, the model of the roadway strain on the circular hole, shown in Figure 4 below, is established, and the model's boundary conditions are as follows: the internal geometric boundary is a circular hole with a radius of r_0; P_X and P_Z are the horizontal and lead stresses, respectively, in the regional stress field under the state of the original rock stress, which are both the dominant stresses; and the stress boundary of the circular hole's internal boundary is the branching resistance, but since the roadway support resistance is much smaller than the original rock stress, it can be neglected.

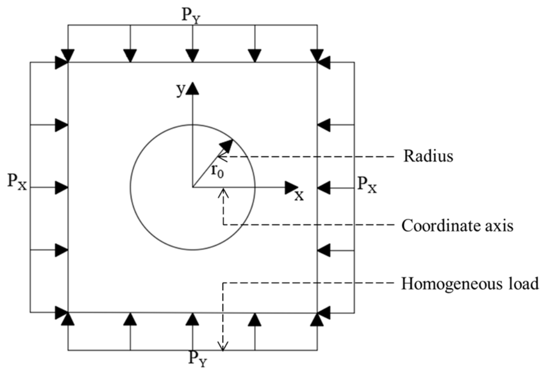

Figure 4. Mechanical model of the perimeter rock of the circular tunnel.

According to the theory of elastic mechanics, the polar coordinate expression for the stress solution at any point of the circular hole enclosure is

$$\begin{cases} \sigma_r = \frac{P_Y+P_X}{2}(1-\frac{r_0^2}{r^2}) + \frac{P_Y-P_X}{2}(1-4\frac{r_0^2}{r^2}+3\frac{r_0^4}{r^4})\cos 2\theta \\ \sigma_\theta = \frac{P_Y+P_X}{2}(1+\frac{r_0^2}{r^2}) - \frac{P_Y-P_X}{2}(1+3\frac{r_0^4}{r^4})\cos 2\theta \\ \tau_{\tau\theta} = \frac{P_Y-P_X}{2}(1+2\frac{r_0^2}{r^2}-3\frac{r_0^4}{r^4})\sin 2\theta \end{cases}, \tag{1}$$

where σ_r is the radial stress at any point outside the circular borehole, σ_θ is the circumferential stress, $\tau_{r\theta}$ is the shear stress, (r, θ) is the polar coordinates of any point, r_0 is the radius of the roadway, P_Y is the vertical stress, and P_X is the horizontal stress.

There is also the conversion relation between the stress expression in elastic mechanics in the right-angle coordinate system and the stress expression in the polar coordinate system there:

$$\begin{cases} \sigma_x = \frac{\sigma_r+\sigma_\theta}{2} + \frac{\sigma_r-\sigma_\theta}{2}\cos 2\theta - \tau_{r\theta}\sin 2\theta \\ \sigma_x = \frac{\sigma_r+\sigma_\theta}{2} - \frac{\sigma_r-\sigma_\theta}{2}\cos 2\theta + \tau_{r\theta}\sin 2\theta \\ \tau_{xy} = \frac{\sigma_r-\sigma_\theta}{2}\sin 2\theta + \tau_{r\theta}\cos 2\theta \end{cases}, \tag{2}$$

The expressions for the maximum and minimum principal stresses at any point in elastic mechanics are

$$\begin{cases} \sigma_1 = \frac{\sigma_x+\sigma_y}{2} + \frac{1}{2}\sqrt{(\sigma_x-\sigma_y)^2+4\tau_{xy}} \\ \sigma_3 = \frac{\sigma_x+\sigma_y}{2} - \frac{1}{2}\sqrt{(\sigma_x-\sigma_y)^2+4\tau_{xy}} \end{cases}, \tag{3}$$

where σ_1 is the maximum principal stress and σ_3 is the minimum principal stress.

The polar coordinate expressions for the maximum and minimum principal stresses at any point within the surrounding rock can be obtained by combining Equations (2) and (3):

$$\begin{cases} \sigma_1 = \frac{\sigma_r+\sigma_\theta}{2} + \sqrt{(\frac{\sigma_r-\sigma_\theta}{2})^2+(\tau_{r\theta})^2} \\ \sigma_3 = \frac{\sigma_r+\sigma_\theta}{2} - \sqrt{(\frac{\sigma_r-\sigma_\theta}{2})^2+(\tau_{r\theta})^2} \end{cases}, \tag{4}$$

It is also known from the Moorcullen damage criterion that the limiting damage condition of the tunnel envelope is

$$\sigma_1 = 2C\frac{\cos\varphi}{1-\sin\varphi} + \frac{1+\sin\varphi}{1-\sin\varphi}\sigma_3, \tag{5}$$

Therefore, substituting Equation (4) into Equation (3) yields an expression for the surrounding rock stress at a point in the roadway:

$$\frac{2+\sin\varphi}{2-2\sin\varphi}\sqrt{(\sigma_r-\sigma_\theta)^2+4\tau_{r\theta}^2} - 2C\frac{\cos\varphi}{1-\sin\varphi} - \frac{\sigma_r+\sigma_\theta}{2}\frac{3\sin\varphi}{1-\sin\varphi} = 0, \tag{6}$$

Substituting Equation (2) into Equation (5) and associating it with Equation (3) yields the implicit equation for the boundary of the plastic zone of the circular roadway enclosure:

$$\begin{cases} \frac{2+\sin\varphi}{2-2\sin\varphi}\sqrt{\left[(1+k)P_Y\frac{r_0^2}{r^2}+2(k-1)P_Y\cos 2\theta\frac{r_0^2}{r^2}\right]^2+4\left[\frac{(1-k)P}{2}\left(1+2\frac{r_0^2}{r^2}-3\frac{r_0^2}{r^4}\right)\sin 2\theta\right]^2} \\ -2C\frac{\cos\varphi}{1-\sin\varphi}+\frac{2(1+k)P_Y\frac{r_0^2}{r^2}}{2}\times\frac{3\sin\varphi}{1-\sin\varphi}=0 \end{cases}, \tag{7}$$

3.2. Characterization of the Plastic Zone of the Base Plate Surrounding the Rock

The role of the bottom-pumping roadway is mainly to extract gas from the working face above, so it needs to be considered when determining the reasonable longitudinal layer of the bottom-pumping roadway. ① Article 21 of the Measures for Preventing Coal and Gas Outbursts stipulates that the roadway less than 10 meters away from the prominent coal seam must be excavated while exploring and the distance between the roadway and the coal seam must be ensured to be not less than 5 m. Therefore, in determining the longitudinal layer of the bottom-pumping roadway, it must be ensured that the bottom-pumping roadway roof from the coal seam above the distance of the cloth is less than 10 m [31]. ② To satisfy the use of gas-extraction equipment in the bottom roadway, the section size of the bottom roadway of the Licun coal mine is designed to be 5000 mm × 4000 mm in width × height. Combined with these two relevant provisions, and according to the rock stratum column diagram of the Licun coal mine, the main rock layers of the coal seam floor are found to be sandy mudstone, fine-grained sandstone, siltstone, mudstone, medium-grained sandstone, and limestone. In addition, the distance from the coal seam floor to the limestone is found to be 15 m. It can be seen that with the less optimal bottom-pumping roadway at the bottom of the longitudinal layer of the floor, along with the limestone lithology of the harder endowment of the stability of the bottom of the pumping roadway arranged in the limestone formation, the roadway excavation is bound to increase labor, and the bottom-pumping roadway arranged at the bottom of the roadway will also increase labor. If the bottom-pumping roadway is arranged in the limestone rock layer, the roadway excavation will certainly increase the amount of labor, and if it is arranged below the bottom-pumping roadway, the amount of drilling work will also increase when the bottom-pumping roadway is subsequently drilled for extraction. Therefore, the comprehensive consideration is to arrange the bottom-pumping tunnel above the limestone, i.e., along the medium-grained sandstone, which can not only maintain the stability of the bottom plate of the bottom-pumping tunnel but also ensure the safety distance between the bottom-pumping tunnel and the coal seam.

From the geological data of Licun coal mine 3301's working face, the buried depth of medium-grained sandstone is 540 m, i.e., the vertical stress above the bottom-pumping lane is 1.35 MPa. The designed section size of the bottom-pumping lane is width × height = 5000 mm× 4000 mm, i.e., its radius is 2.5 m. Finally, from the above physical and mechanical experiments of the surrounding rock, it can be seen that the cohesion of the medium-grained sandstone is 1.25 MPa, and the angle of internal friction is 20°. According to related scholars [32], $\frac{104}{h}+0.75<k<\frac{265}{h}+0.98$. According to the expression of the distribution law of ground stress with burial depth, it can be known that the value range of the pressure coefficient of the bottom-pumping tunnel is 0.95–1.47, and k = 1.4 for the convenience of the study, so it can be known that the horizontal stress of the surrounding rock under the original rock stress condition of the bottom-pumping tunnel is Px = 1.89 MPa.

Due to the mining in the working face, the bottom plate is affected by the mining of the stress redistribution in the surrounding rock, the formation of a nonuniform stress field in the bottom plate of the working face, and the two-way stress ratio of the surrounding rock; these are obvious differences [33]. The two-way stress ratio of the surrounding rock shows obvious differences, and the bottom-pumping lane is arranged in the rock layer of the bottom plate. Its two-way stress ratio is bound to be different under the influence of the mining of the working face. Therefore, to analyze the bottom-pumping lane with different bidirectional stress ratios under the surrounding rock's plastic-zone damage characteristics, with the original rock stress's bidirectional stress ratio k = 1.4 as the dividing line, we take k = 1.0, 1.5, 2.0, 2.5, 3.0, which can be obtained from the bottom-pumping lane surrounded by the plastic zone damage characteristics of the plastic zone, as shown in Figure 5.

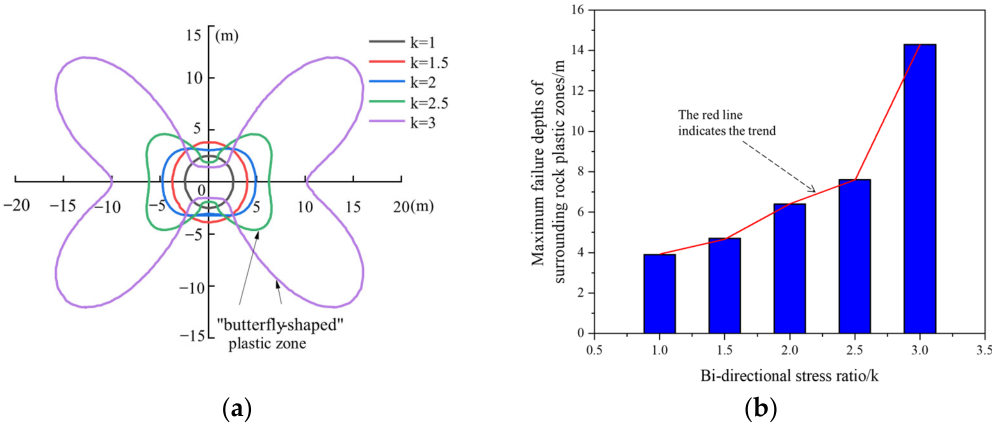

Figure 5. Distribution characteristics of the plastic zone of the roadway's surrounding rock under different bidirectional stress ratios: (**a**) distribution curve of the plastic zone of surrounding rock; (**b**) distribution characteristics of the plastic zone of surrounding rock.

From Figure 5a, different two-way stress ratios under the roadway surrounding the rock plastic zone boundary curve can be seen. With the gradual increase in the two-way stress ratio k, the shape of the roadway surrounding the rock plastic zone presents obvious characteristics of a circular–elliptical–butterfly-shaped morphology change, and the surrounding rock plastic zone has "butterfly" plastic zone morphology characteristics. The expansion of the surrounding plastic zone with the two-way stress ratio has a strong sensitivity to the expansion of the plastic zone, i.e., with the increase in the two-way stress ratio, the expansion of the plastic zone is more obvious. When the plastic zone of the surrounding rock reaches the "butterfly-shaped" plastic zone, the expansion of the plastic zone of the surrounding rock has a strong sensitivity to the bidirectional stress ratio, i.e., the expansion of the plastic zone of the surrounding rock becomes more and more obvious with the increase in the bidirectional stress ratio. Combined with Figure 5b, different bidirectional stress ratios of the surrounding rock's plastic zone damage area can be seen, with a bottom-pumping lane in the bidirectional stress ratio of the larger nonuniform stress field. Furthermore, the plastic zone damage area is significantly larger than the bidirectional stress ratio of the smaller nonuniform stress field of the plastic zone's damaged area. It can be seen that the bidirectional stress ratio of the larger nonuniform stress field is a serious threat to the bottom of the pumping lane surrounding the stability of the rock. Among the conditions, k = 1 is the most ideal, and the degree of damage to the roadway is the smallest. As the bottom-pumping lane is arranged below the bottom plate of the working face, when the working face is mined and affected by the mining of the working face, it is bound to experience a variety of nonuniform stress fields, so choosing a reasonable location for the bottom-pumping lane and preventing it from experiencing a large nonuniform stress field are the key to maintaining the stability of the perimeter rock of the bottom-pumping lane.

4. Distribution Law of Floor Stress and Bidirectional Stress Ratio in the Working Face

From the above analysis, it can be seen that the damage characteristics of the plastic zone of the surrounding rock are mainly determined by the stress environment in which it is located, and the damage characteristics of the surrounding rock under different bidirectional stress ratios have obvious differences. In addition, under the influence of mining, the bidirectional stress ratios are bound to be different in different locations of the bottom plate of the working face. Therefore, the distribution of bidirectional stress ratios is the key to determining the reasonable location of the bottom-pumping roadway. The numerical simulation of the bottom plate after mining is analyzed using FLAC^{3D} to analyze the distribution characteristics of the bidirectional stress ratios. In this section, FLAC^{3D} numerical simulation is used to analyze the distribution characteristics of the two-way stress ratio in the surrounding rock of the bottom plate after mining to determine the reasonable location of the bottom-pumping roadway.

4.1. Modeling

According to the geological engineering conditions of the Licun coal mine, the length of the 3301 working face is 160 m, and the width of the coal pillar protected by the working face is 30 m. To avoid the influence of the boundary effect, the numerical model was established as shown in Figure 6 below, and the size of the model was 360 m × 420 m × 200 m. The intrinsic Mohr–Coulomb model was adopted for the model. In addition, horizontal displacement constraints were applied on both sides and the front and rear boundaries, vertical displacement constraints were applied on the bottom boundary, and uniformly distributed loads were applied on the upper boundary of the model. The load set degree was determined to be 13 MPa based on the depth of the burial of the coal seam, and the physical and mechanical parameters of each rock stratum from the rock mechanical parameters shown in Table 1 were adopted.

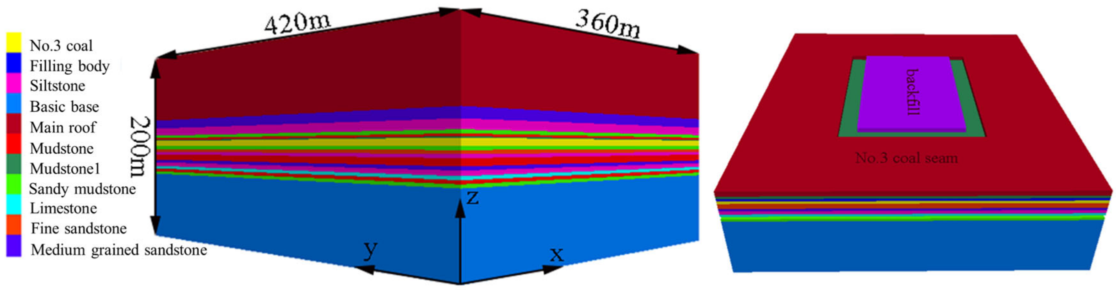

Figure 6. Numerical model diagram.

Through on-site research, we learned that the step interval of 3301's working face with cycle pressure was 20 m, and the step interval of the initial pressure was 38 m. The simulation corresponded to the real situation in the field, and to make the stress of the working face's top plate transfer to the bottom plate in the hollow area, we simulated the recovery of the bottom plate stress in the hollow area after the initial pressure of the working face and the cycle pressure. Therefore, we determined that the working face must be excavated as follows. The model was excavated along the x-axis for 160 m to simulate the length of the working face, and from the position of the y-axis at 100 m, the excavation was carried out in 12 steps, with an excavation interval of 20 m, and a total of 240 m was excavated. Then, after the third step of the excavation of the working face, the filling body of length × width × height = 120 m × 20 m × 6 m was filled at the lagging position of the working face, which was simulated using the double yield model, and its physical and mechanical parameters are listed in Table 2 below, including the simulation and its physical and mechanical parameters.

Table 2. Physical and mechanical parameters of the filling body.

Name of Rock Formation	Density/kg·m^{-3}	Bulk/GPa	Shear/GPa	Friction Angle/(°)	Tensile Strength/MPa	Resistance Max/MPa
filling body	2000	4.3556	0.068	32	0.1	0

4.2. Validation of the Reasonableness of the Numerical Simulation

From the above distribution, it can be seen that the bottom-pumping roadway is arranged in the medium-grained sandstone of the bottom plate of the working face, and the distance from the working face is 15 m. Therefore, the vertical stress cloud map at the position of 15 m of the bottom plate of the working face is intercepted as shown in Figure 7 below. The vertical stress of monitoring line 1 is arranged in the middle of the position of 15 m at the bottom plate of the working face, and the stress monitoring curve of the vertical stress monitoring line is extracted as shown in Figure 8 below.

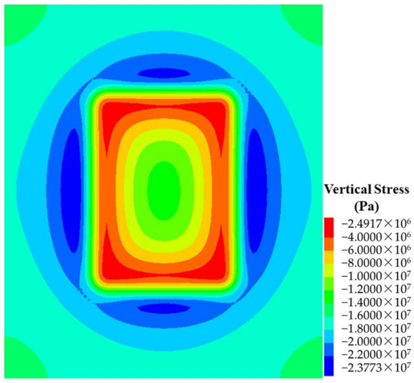

Figure 7. Vertical stress cloud at 15 m on the bottom plate of the working face.

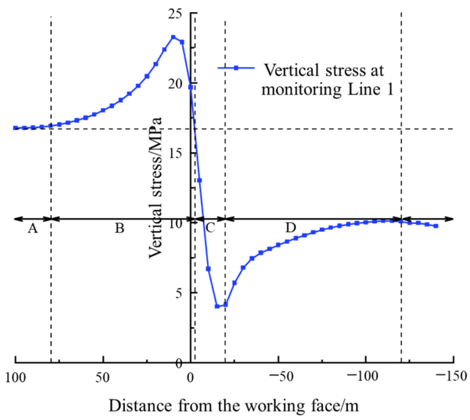

Figure 8. Vertical stress distribution curve of monitoring line 1.

According to the vertical stress cloud diagram at 15 m on the bottom plate of the working face in Figure 7, it can be seen that within the projection range of the coal pillar outside the hollow area, the vertical stress appears to be a stress-concentration phenomenon, the vertical stress of the surrounding rock outside the filling area at the edge of the projection of the hollow area decreases greatly, the vertical stress of the surrounding rock in the range of the filling area is gradually restored, and the closer to the middle of the hollow area, the better the effect of the vertical stress. Combined with the vertical stress distribution curve of monitoring line 1 in Figure 8, it can be seen that the vertical stress of the surrounding rock in the range of 80 in front of the working face increases gradually, the vertical stress reaches a maximum of 23.5 MPa at the position of 10 m in front of the working face, the vertical stress decreases sharply in the range of 23 m behind the working face, the vertical stress reaches a minimum of 3.6 MPa at this position, the vertical stress gradually increases in the range of 24–100 m behind the working face, and the vertical stress decreases gradually in the range of 24–100 m behind the working face. In the range of 24–100 m behind the working face, the vertical stress of the surrounding rock increases gradually, and the vertical stress of the surrounding rock stays above and below 11 MPa. Therefore, the vertical stress from the edge of the model to the middle of the mining area can be divided into the original rock stress area, the stress increase area, the stress decrease area, and the stress stabilization area, and its change is in line with the distribution law of the supporting pressure of the working face's bottom plate after the coal seam is mined [34]. The change occurs due to the distribution of support pressure in the working face after mining, which verifies the accuracy of the numerical simulation.

4.3. Characteristics of the Bidirectional Stress Ratio Distribution of the Bottom Plate of the Working Face

Vertical and horizontal stress monitoring lines 2, 3, and 4 were arranged in the middle of the working face (Figure 9), and the distance from the working face is 15 m, the distance to the right of the middle of the working face is 40 m, and the distance outside the projection of the coal pillar is 15 m. The monitoring lines all went along the normal direction of the working face, and the distribution of the peripheral rock stress and the bidirectional stress ratio at different locations of the bottom plate of the working face were obtained as shown in Figure 10.

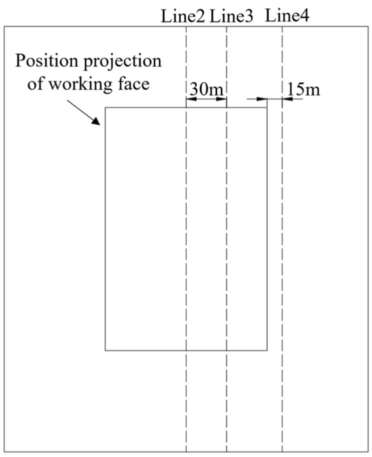

Figure 9. Line layout diagram.

According to the monitoring curve of the stress and the bidirectional stress ratio at different locations in Figure 10, it can be seen that when the vertical stress increases sharply, the horizontal stress increases slightly, and when the vertical stress decreases sharply, the horizontal stress decreases less, which means that that there is a weakly sensitive feature of the vertical stress and the horizontal stress of the surrounding rock at the bottom plate of the working face. Therefore, due to the existence of this weak sensitivity, the two-way stress ratio of the surrounding rock changes drastically at different locations of the base plate.

The monitoring line 2 stress and bidirectional stress ratio monitoring curve can be seen in Figure 10a. In the area far away from the mining range (0–60 m), the surrounding rock is in the original rock stress state, and the bidirectional stress ratio is almost unchanged, so this area is defined as the "original rock stress ratio area". In the area close to the mining range (60–100 m), the vertical stress of the surrounding rock is significantly increased by the mining. In the area near the mining range (60–100 m), the vertical stress of the surrounding rock increases significantly, the horizontal stress increases less, the bidirectional stress ratio decreases from 1 to 0.7, and the surrounding rock is in a pressurized state in this range, so this area is defined as a "pressurized low-stress ratio area". In the mining range (100–140 m), due to the mining of the working face, the surrounding rock is in a decompression state, the vertical stress decreases significantly, and the vertical stress decreases significantly, so this area is defined as an "original rock stress ratio area". In the mining range (100–140 m), due to the mining of the working face, the surrounding rock is in an unpressurized state, and the vertical stress decreases greatly, but the horizontal stress decreases less. At this time, the bidirectional stress ratio increases from 1 to 3.5, and the bidirectional stress ratio is larger. Therefore, this area is defined as the "unpressurized high-stress ratio zone". In the mining range (140–260 m), due to the top plate of the working face collapsing and compacting, the stress in the top plate is transferred downward, and the vertical stress in the bottom plate is transferred to the bottom plate. In the mining range (140–260 m), due to the collapse and compaction of the working face roof, the stress on the top plate is transferred downward, and the vertical stress on the bottom plate gradually recovers and tends to stabilize. At this time, the change in bidirectional stress is relatively small, changing from 1.4 to 1.6. Therefore, this tendency is defined as the "unpressurized stress ratio stabilization zone". The distribution of the bidirectional stress ratio is the same in the range of 260–420 m and the range of 0–260 m and will not be described again here.

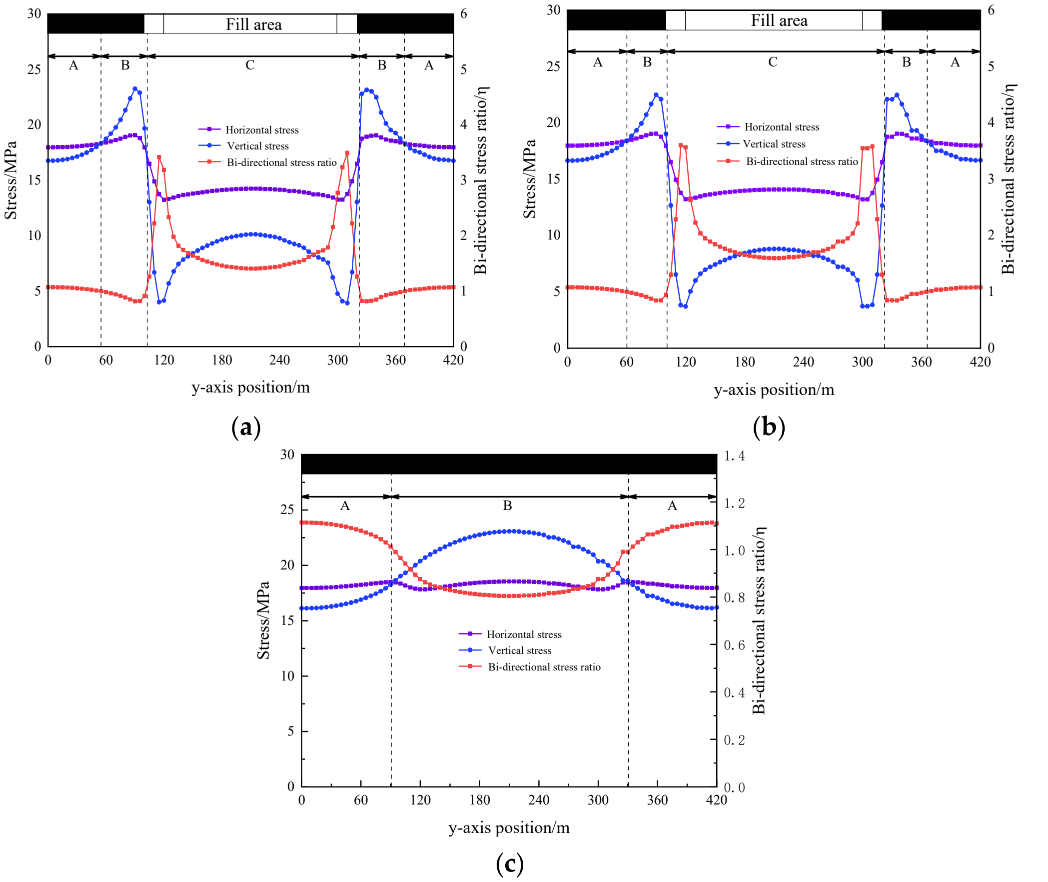

Figure 10. Monitoring curves of stress and bidirectional stress ratios at different locations: (**a**) distribution curve of stress and bidirectional stress ratio for monitoring line 2; (**b**) distribution curve of stress and bidirectional stress ratio for monitoring line 3; (**c**) distribution curve of 4-stress versus bidirectional stress ratios in the monitoring line.

From the monitoring curve of stress and the bidirectional stress ratio in monitoring line 3 in Figure 10b, it can be seen that the distribution law of the bidirectional stress ratio in the surrounding rock is similar to that in monitoring line 2, and there are the "original rock stress ratio zone", "pressurized low-stress ratio zone", "unpressurized high-stress ratio zone" and "unpressurized stress ratio stable zone" from the edge of the model to the mining area. The only difference between monitoring line 2 and monitoring line 3 is that the distribution range of the "unloading stress ratio stabilization zone" is smaller. The distribution range of monitoring line 3's "unpressurized stress ratio stabilization zone" is smaller, and the bidirectional stress ratio is larger.

As shown in Figure 10c, showing the monitoring line 4 stress and bidirectional stress ratio distribution curve, we can see that in the range of 0–90 m, the surrounding rock is in the original rock stress state, and the bidirectional stress ratio of the surrounding rock varies between 1.05–1.1, so this area is called the "original rock stress ratio area". In the range of 90–330 m, the vertical stress is significantly increased by the mining influence, but the horizontal stress increases less, and the bidirectional stress ratio increases from 0.8 to 1.0, so the bidirectional stress ratio is smaller and this area is the "pressurized low-stress ratio area". In the range of 90–330 m, the vertical stress is increased by mining, but the increase in horizontal stress is small, and the bidirectional stress ratio increases from 0.8 to 1.0, which is a small bidirectional stress ratio, so this area is called the "pressurized low-stress ratio area". In the range of 330–420 m, the surrounding rock is in the state of original rock stress, and the bidirectional stress ratio of the surrounding rock varies between 1.05–1.1, so this area is also called the "original rock stress ratio area". Therefore, this area is also called the "original rock stress ratio area". In the range of 330–420 m, the surrounding rock is in the original rock stress state, and the two-way stress ratio of the surrounding rock varies from 1.05 to 1.1, so this area is also the "original rock stress ratio area".

4.4. Characteristics of the Distribution of the Bidirectional Stress Ratio of the Working Face Floor under Distributed Excavation

The above analysis shows that when the bottom-pumping tunnel is arranged below the mining area, the bottom-pumping tunnel will experience the influence of the "original rock stress ratio area", the "pressurized low-stress ratio area", the "unpressurized high-stress ratio area", and the "unpressurized stress ratio stabilization area". If the bottom-pumping roadway is arranged under the coal pillar, it will only experience the influence of the "original rock stress ratio zone" and the "pressurized low-stress ratio zone". To analyze the influence of the bidirectional stress ratio on the bottom-pumping tunnel during the whole excavation process, the vertical and horizontal stresses after excavation are extracted from monitoring line 2, monitoring line 3, and monitoring line 4, and the distribution of the bidirectional stress ratio under excavation is obtained from different locations of the bottom plate of the working face, which is shown in Figure 11 below.

In Figure 11, it can be seen that the bidirectional stress ratios of the surrounding rock under a distributed excavation are completely different at different locations below the floor of the working face.

At monitoring line 2, before the initial pressure, the rock surrounding the bottom plate experiences the environment with the largest bidirectional stress ratio in the whole process of advancing the working face, and after the initial pressure, the bidirectional stress ratio of the surrounding rock will gradually change from a "single-peak-like" to a "double-peak-like" state, and the rock body at a depth of 50 m from the projection of the cutting eye will experience the influence of an "unpressurized high-stress ratio" during the advancing process of the working face, and it will finally be under the influence of the "unpressurized stress ratio stabilization zone".

At monitoring line 3, like at monitoring line 2, the rock surrounding the bottom plate will experience the stress environment with the largest bidirectional stress ratio in the whole process of the advancement of the working face before the initial pressure, and after the initial pressure, the bidirectional stress ratio of the surrounding rock will gradually change from a "single-peak-shape" distribution to a "double-peak-shape" distribution, and the surrounding rock will experience the influence of the "unpressurized stress ratio stabilization zone" in the process of the advancement of the working face. After the initial pressure, the bidirectional stress ratio of the surrounding rock will gradually change from a "single-peaked" distribution to a "bimodal" distribution, and the surrounding rock will experience the influence of the "unpressurized stress ratio stabilization zone" during the process of the advancement of the working face. However, what is different from the bidirectional stress ratio at monitoring line 2 is that during the advancement of the working face, the surrounding rock is located in a stress environment where the bidirectional stress ratio ranges from 2 to 9, with a larger value of the bidirectional stress ratio.

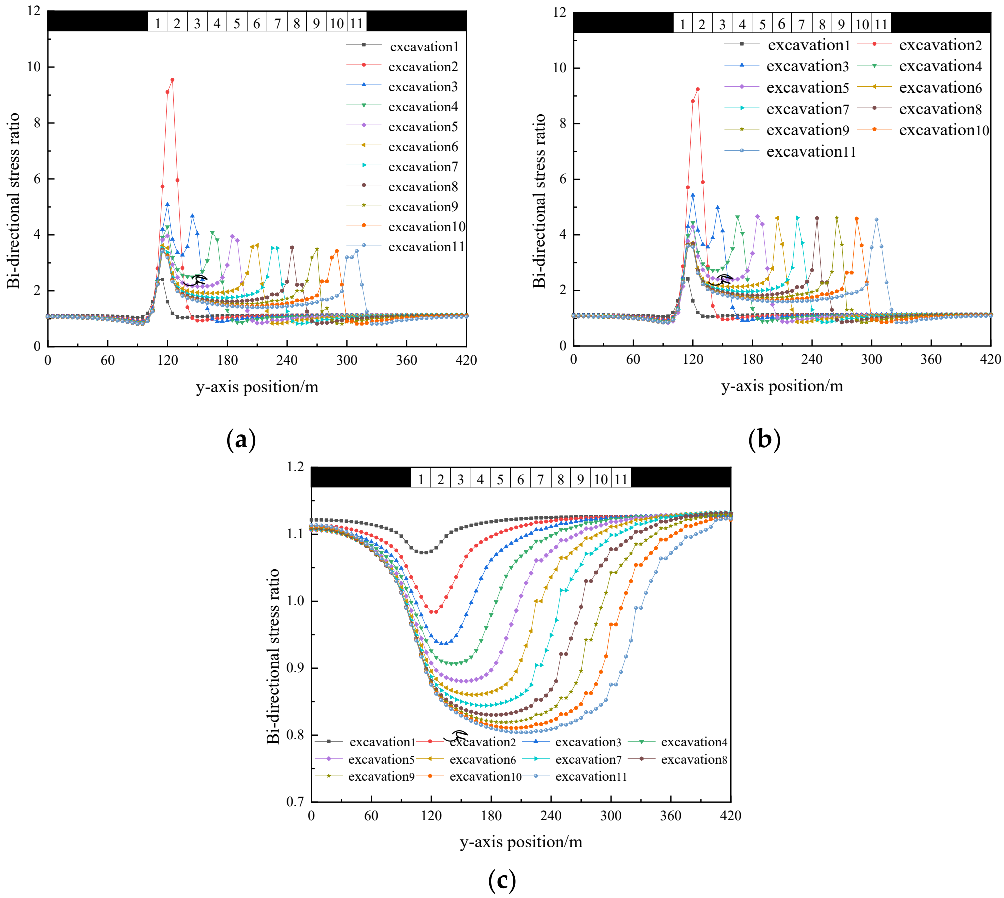

Figure 11. Bidirectional stress ratios at different locations under a distributed excavation: (**a**) bidirectional stress ratio curve for monitoring line 2; (**b**) bidirectional stress ratio curve for monitoring line 3; (**c**) distribution of bidirectional stress ratios for monitoring line 4.

At monitoring line 4, as the working face advances, the stress in the surrounding rock of the bottom plate gradually changes from the horizontal stress-led original rock stress to the vertical stress-led pressurized stress, and as the working face advances, the pressurized state of the surrounding rock gradually increases and finally remains stable, and finally, the bidirectional stress ratio of the surrounding rock is maintained at about 0.8. Therefore, in the whole process of working face advancement, the surrounding rock experiences the influence of the "original rock stress ratio area" and "pressurized low-stress ratio area".

As the bottom-pumping roadway is arranged in the rock layer of the bottom plate of the working face, the above analysis shows that when the bottom-pumping roadway is arranged in the middle of the projection of the hollow area, it is affected by the mining movement of the working face and experiences the influence of the "unpressurized high-stress ratio zone" and the "unpressurized stress ratio stabilization zone". When the bottom-pumping tunnel is arranged at the position 40 m to the right of the center of the projection of the hollow mining area, it experiences the influence of a "pressure relief high-stress ratio area" and a "pressure relief stress ratio stabilization area", with a larger bidirectional stress ratio. When the bottom-pumping tunnel is arranged at the position 15 m outside the projection of the mining hollow area below the coal pillar, it only experiences the influence of the "original rock stress ratio area" and the "pressure relief stress ratio stabilization area". When the bottom drawer is arranged below the coal pillar, i.e., 15 m outside the projection of the mining area, it only experiences the influence of the "original rock stress ratio area" and the "pressurized low-stress ratio area". According to the theory of the "butterfly plastic zone" in Section 3, the larger the bidirectional stress ratio is, the larger the surrounding rock plastic zone is. Therefore, it can be seen that when the bottom-pumping roadway is arranged below the coal pillar, i.e., 15 m outside the wrong position of the mining area, the surrounding rock plastic zone is the smallest, and its position is the most reasonable, which is verified by numerical simulation below.

5. Verification of the Reasonable Location of the Bottom-pumping Alley

The three schemes designed are shown in Figure 12. In order to verify the reasonableness of the above location of the bottom-pumping roadway arrangement, the perimeter's rock damage characteristics when the bottom-pumping roadway is arranged at different locations are simulated.

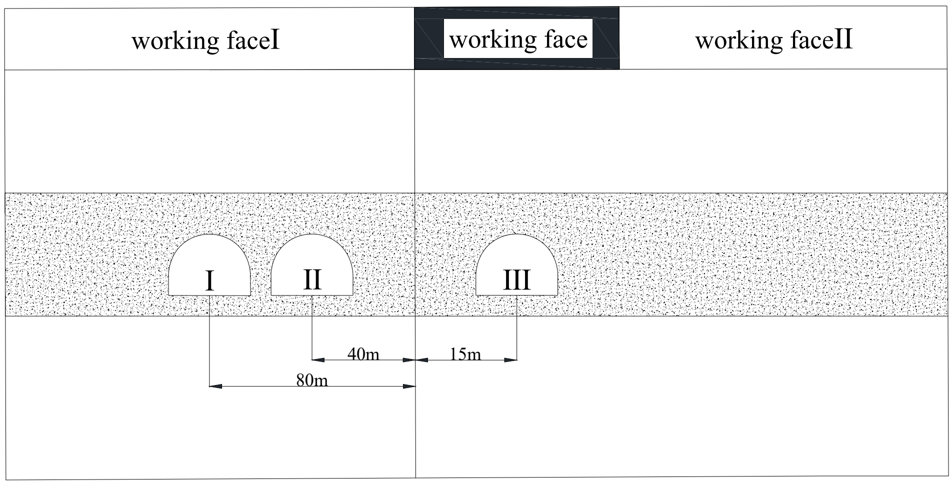

Figure 12. Simulation scheme of the bottom-pumping roadway.

Scheme 1: the bottom-pumping roadway is arranged at the center line of the working face. Scheme 2: the bottom-pumping roadway is arranged at the position 40 m outside the middle of the mining hollow area. Scheme 3: the bottom-pumping roadway is arranged at the position 15 m outside the mining hollow area. Considering the influence of the adjacent back-to-mining of the working face, the 30 m protective coal pillar will be retained after the back-to-mining of working face 1, followed by the back-to-mining of working face 2. The numerical model developed is shown in Figure 13.

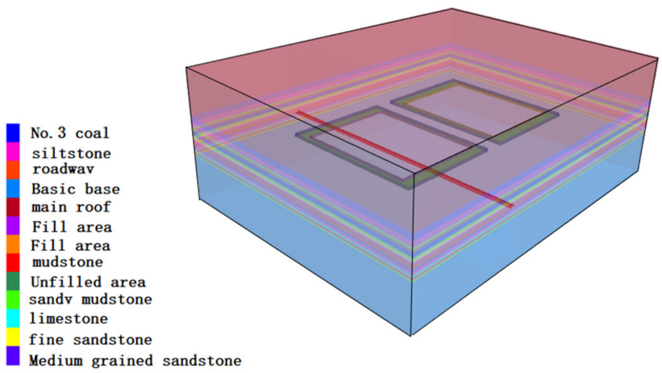

Figure 13. Bottom pumping roadway layout model.

Figure 14 below shows, for each scheme, the interception of the cut at the maximum damage area of the plastic zone of the surrounding rock, which is in the bottom draw roadway of each scheme, along with the statistics of the damaged area of the plastic zone of the surrounding rock in the bottom draw roadway.

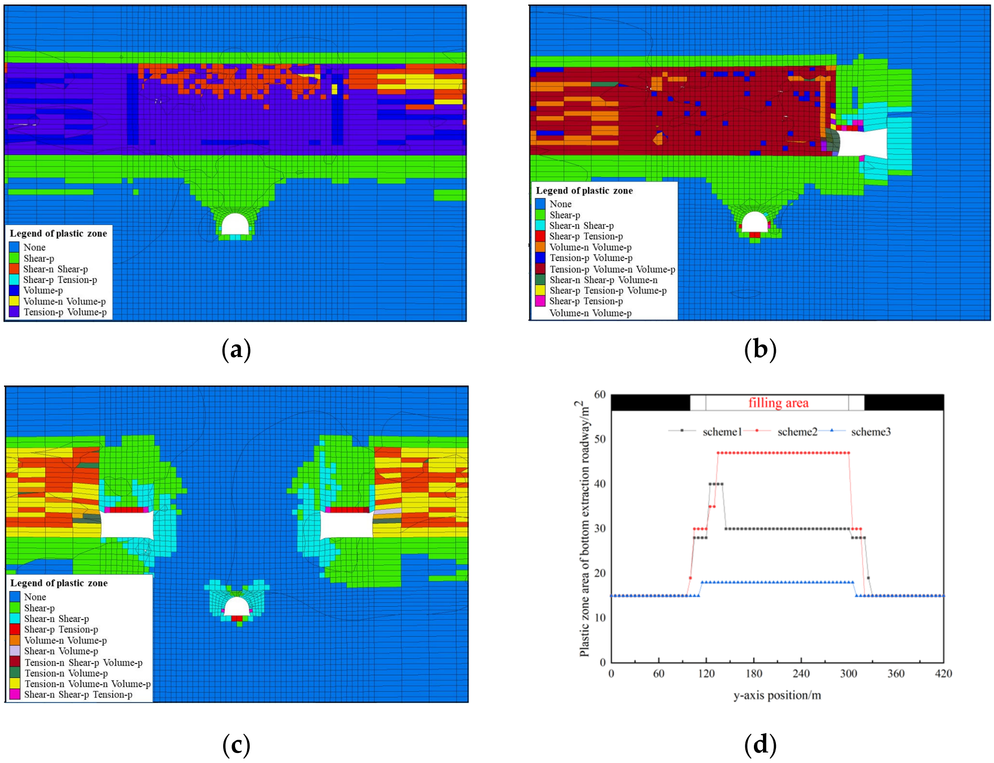

Figure 14. Distribution characteristics of the plastic zone in the bottom-pumping roadway of different schemes and statistics for the area of the plastic zone in the surrounding rock. (**a**) Scheme 1: y = 125 m; (**b**) Scheme 2: y = 220 m; (**c**) Scheme 3: y = 220 m. (**d**) Statistics for the area of the plastic zone of the surrounding rock in the bottom-pumping tunnel.

Figure 14d shows the statistics for the bottom-pumping roadway surrounding the rock plastic area. In the distribution of excavation calculations after the balance, the destruction area of the bottom-pumping roadway surrounding the rock plastic area of each program shows obvious differences. Outside the mining range of the working face, due to the small impact of mining on the working face, the damage area within each program's bottom-pumping row perimeter rock plastic area is 15 m^2. In the mining orientation of the working face, option 2 in the damage area of the bottom-pumping roadway's peripheral rock plastic area appears to increase significantly. In the working face excavation from the opening eye in the range of 20 m–45 m, the damage area within the bottom-pumping roadway peripheral rock plastic area reaches a maximum of 40 m^2. In the range of 20 m from the opening eye and the end mining penetration, the area of the plastic zone of the surrounding rock in the bottom-pumping tunnel is 28 m^2, and the area of the plastic zone of the surrounding rock in the rest of the location of the bottom-pumping tunnel is 30 m^2. In Scheme 1, the damaged area of the plastic zone of the surrounding rock of the bottom-pumping tunnel increases drastically, and the maximum damage area of the surrounding rock of the plastic zone of the bottom-pumping tunnel in the range of 25 m–200 m from the opening eye reaches 47 m^2. In Scheme 3, due to the arrangement of the bottom-pumping tunnel below the coal pillar, the bottom plate rock is affected by the pressurization and by the environment having a low stress ratio, which is the most important factor in the development of the bottom-pumping tunnel. In Scenario 3, due to the layout of the bottom roadway below the coal pillar, the surrounding rock of the bottom slab is affected by the environment being pressurized and having a low-stress ratio, and the plastic zone of the surrounding rock of the bottom roadway is less affected by the mining of the working face. In addition, the damaged area of the surrounding rock plastic zone is the smallest, and the damaged area of the surrounding rock plastic zone of the bottom drawway is only 18 m within the mining range of the working face^2. Finally, the damaged area of the surrounding rock plastic zone of the bottom roadway is the same as those of Scenarios 1 and 2, which are both 15 m^2. Combined with the different locations of the graphs in Figure 14a–c, it can be seen that the destructive characteristics of the plastic zone of the surrounding rock in the bottom-pumping tunnel, the destructive range of the plastic zone of the surrounding rock in the bottom-pumping tunnel of Scheme 1 and Scheme 2 are connected to the destructive range of the plastic zone of the bottom plate of the open area. It can also be seen that the destructive range of the plastic zone of the surrounding rock in the bottom-pumping tunnel of Scheme 3 is not connected with the plastic zone of the bottom plate of the open area of the two sides. In Scheme 1 and Scheme 2, two arrangement schemes of the bottom-pumping roadway peripheral rock are always affected by the unloading pressure at a high-stress ratio range. In addition, the bottom-pumping roadway peripheral rock plastic area under the mining air zone damaged area is large, and the roadway's top plate plastic area and the bottom plate of the mining air zone are connected to the plastic area. Scheme 3 in the bottom-pumping roadway is affected by the pressurized stress environment, but the bottom-pumping roadway is far from the peripheral rock stress concentration area, the bottom-pumping roadway peripheral rock is always in the pressurization of the low-stress ratio environment, the damaged area within the peripheral plastic area is small, and the bottom-pumping roadway is not connected with both sides of the mining air zone plastic area. At the same time, there is a large intact rock layer between the plastic zone of the top plate of the bottom-pumping roadway and the plastic zone of the bottom plate of the hollow area, which ensures the stability of the surrounding rock of the bottom-pumping roadway. Therefore, according to the degree of influence on the stability of the peripheral rock in the bottom-pumping tunnel, the order of the four stress states is depressurized high-stress ratio area > depressurized stress ratio stable area > pressurized low-stress ratio area > original rock stress ratio area. Therefore, the reasonable location of the bottom-pumping tunnel is 15 m below the coal pillar, which is the most reasonable location outside the mining area, and the correctness of the numerical analysis in Section 4 is also verified.

6. Field Application and Effect Analysis

The results of the above analysis show that the reasonable location of the bottom-pumping roadway in the working face of Licun coal mine 3301 is below the coal pillar and dug along the limestone roof plate. The roadway is supported by anchor rods + anchor cable joint support, the row spacing between anchor rods is 900 mm × 1400 mm, and the row spacing between anchor cables is 2400 mm × 1400 mm; the supporting schematic diagram is shown in Figure 15 below.

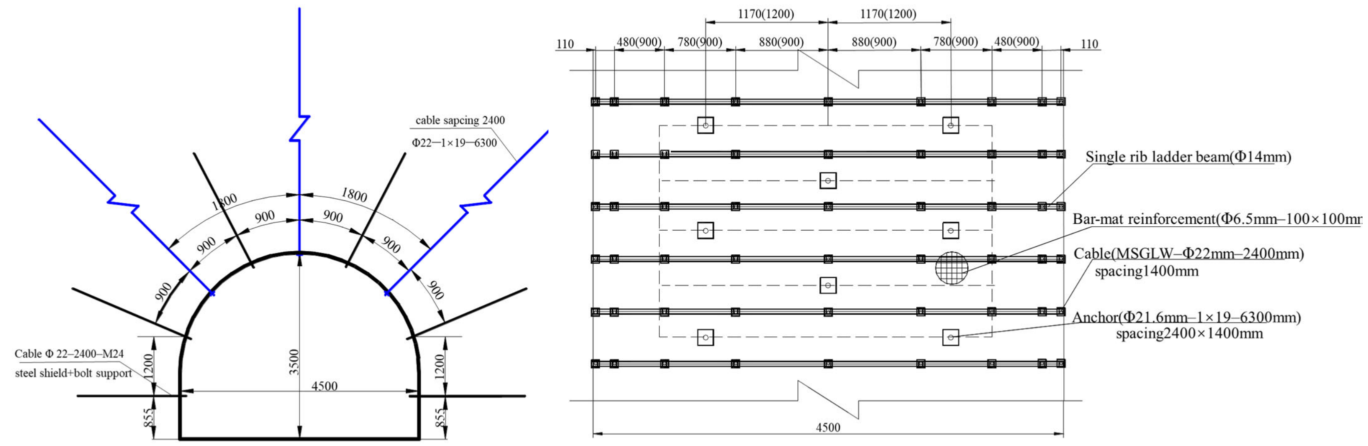

(**a**) (**b**)

Figure 15. Schematic diagram of the bottom draw alley support: (**a**) cross-section of bottom drawer support; (**b**) plan view of bottom drawer support.

The real-time monitoring of the deformation of the surrounding rock and the force of the anchor rods and cables in the bottom-pumping roadway was carried out in a range of 200 m, and the monitoring results are shown in Figure 16 below.

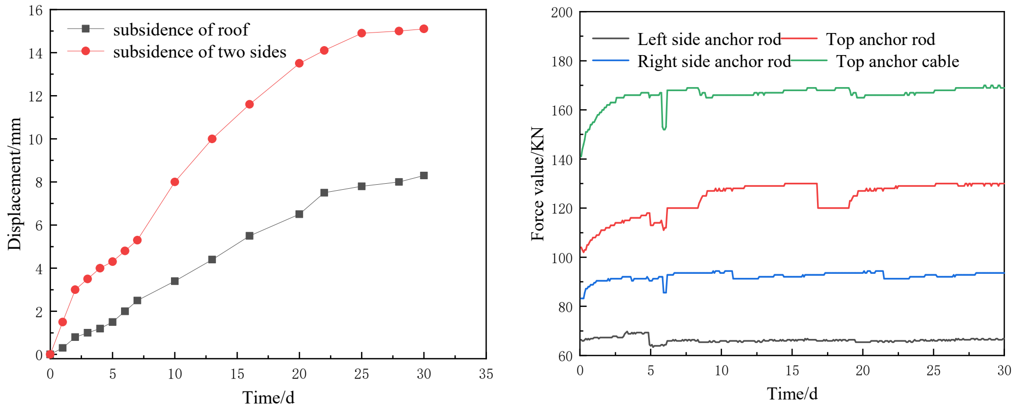

(**a**) (**b**)

Figure 16. Deformation of the surrounding rock in the bottom-pumping roadway and the force on the anchor rods and anchors: (**a**) deformation of the roadway perimeter rock; (**b**) strength of the anchor rods and cables.

According to the monitoring results, the maximum value of the roadway roof subsidence is 9 mm. When the deformation of the two sides and the roof and floor of the roadway does not exceed 10% of the designed section size of the roadway, the roadway can serve normally. The monitoring results show that the actual roadway deformation is less than 1%, the maximum value of the two gangs approaching is 16 mm, the deformation of the roadway is larger within 0~20 d, and the deformation of the roadway is smaller. The deformation rate is low after 20 d, and the peripheral rock of the roadway remains stable. The roadway gradually slows down the deformation rate at 120 m from the headland (the slope rate becomes smaller). The roadway is stabilized 170 m away from the headland, and the anchor rods and anchor cables are subjected to synchronous force during the deformation of the peripheral rock. Furthermore, anchor rods and an anchor cable in the peripheral rock experience a deformation synchronization force, and the overall force presents the first increase after the trend of stability. When the force of the anchor cable is less than 50% of the initial force, the support effect is considered to be lost. At this time, the anchor rods and anchor cable have a role in the roadway above the peripheral rock, limiting its overall displacement and interlayer misalignment. The formation of the peripheral rock and the support community give full play to the role of the anchor rods and the anchor cable support. They also support the deformation of the roadway peripheral rock, which does not increase significantly after the whole is in a stable state. This proves that the choice of the location of the bottom draw and the support program design is reasonable.

7. Discussion

At present, the layout method of bottom-drainage roadways mainly includes theoretical analysis and empirical methods. In terms of theoretical calculation, due to the simplification of relevant specific mining and geological conditions in the calculation process, there is a certain deviation between the final results and the actual situation. The empirical method is strongly constrained by the testing conditions, the actual deviation is very large, and it is even easy for engineering accidents to occur. Therefore, the method of combining theory with numerical simulation is used to study the layout of the bottom-drainage roadway. This method is not limited by specific mining conditions and has strong applicability. The collection of rock data involved in this method is also relatively easy. However, it is necessary to point out that for numerical simulation, because it is difficult to select accurate parameters when establishing numerical models, there is a certain deviation in reflecting the actual situation on site. Therefore, the feasibility of the method should be verified through subsequent engineering practices and further improved and optimized.

8. Conclusions

(1) In the nonuniform stress field under the influence of mining in the upper working face, and with the increase in the bidirectional stress ratio, the damage characteristics of the roadway surrounding the rock show the characteristics of a "butterfly" nonuniform distribution, and the "butterfly" nonuniform damage to the rock surrounding the roadway significantly reduces the stability of the rock surrounding the roadway.

(2) The working face of 3301 is mainly for the mining of No. 3 coal, and its roof is dominated by dark gray mudstone and sandy mudstone, while the floor is mainly black mudstone and sandy mudstone. After the excavation of the working face, according to the size of the two-way stress ratio and the state of the loading and unloading of the surrounding rock stress, the floor of the coal bed can be divided into four kinds of stress states, namely "original rock stress ratio area", "unloading high-stress ratio area", "pressurized low-stress ratio stable area", and "pressurized high-stress ratio area". When the bottom drawer is arranged below the working face, it will experience an "unloading high-stress ratio area" and a "pressurized low-stress ratio stable area". When the bottom-pumping road is arranged below the working face, it will experience an "unpressurized high-stress ratio zone" and an "unpressurized stress ratio stability zone". When the bottom-pumping tunnel is arranged below the working face, it will experience the influence of a "decompression high-stress ratio area" and a "decompression stress ratio stabilization area". When the bottom-pumping tunnel is arranged below the coal pillar, it will experience the influence of a "pressurized low-stress ratio area".

(3) The theory of the "butterfly shape" of the plastic zone indicates that the reasonable location of the bottom-pumping roadway is 15 m below the coal pillar. The damage range and deformation characteristics of the plastic zone at different locations of the bottom-pumping tunnel in the coal seam bottom plate are in the following order: "unpressurized high-stress ratio zone" > "unpressurized stress ratio stable zone" > "pressurized low-stress ratio zone" > "original rock stress ratio zone", which verifies the reasonableness of the bottom-pumping roadway arranged at the 15 m position outside the faulty hollow area below the coal pillar.

(4) Industrial experiments show that the bottom-pumping roadway is arranged in the coal pillar below the hollow area outside the wrong 15 m. Along where the digging of the limestone roof plate is carried out, the maximum value of the roof sinks by 9 mm, the maximum value of the two gangs approaches 16 mm, the deformation of the roadway's perimeter rock is in a reasonable range, and the location of the bottom-pumping roadway has a reasonable layout.

Author Contributions: Conceptualization, L.B. and F.W.; methodology, B.L.; software, P.Y. and S.Z.; validation, P.Y.; formal analysis, L.B.; investigation, L.B.; data curation, B.L.; writing—original draft preparation, L.B.; writing—review and editing, L.B., P.Y. and F.W.; visualization, L.B., P.Y., S.Z. and F.W.; funding acquisition, F.W. All authors have read and agreed to the published version of the manuscript.

Funding: This research received no external funding.

Institutional Review Board Statement: Not applicable.

Informed Consent Statement: Not applicable.

Data Availability Statement: The data presented in this study are available in article.

Conflicts of Interest: Author Libin Bai was employed by the company Liuta Coal Mine, China National Energy Shendong Coal Group.The remaining authors declare that the research was conducted in the absence of any commercial or financial relationships that could be construed as a potential conflict of interest.

References

1. Sotskov, V.; Dereviahina, N.; Malanchuk, L. Analysis of operation parameters of partial backfilling in the context of selective coal mining. *Min. Miner. Depos.* **2019**, *13*, 129–138. [CrossRef]
2. Wu, F.F.; Zhang, S.R.; Yue, X.; Liu, C.; Liu, Q.; Zhang, J.; Lv, B.; Gao, Z. Study on mechanism and improvement technology of Top coal loss in horizontal sublevel fully mechanized caving mining. *Energy Explor. Exploit.* **2022**, *40*, 1394–1408. [CrossRef]
3. Moomivand, H.; Moosazadeh, S.; Gilani, S.O. A new empirical approach to estimate the ratio of horizontal to vertical in-situ stress and evaluation of its effect on the stability analysis of underground spaces. *Rud.-Geol.-Naft. Zb.* **2022**, *38*, 97–107. [CrossRef]
4. Dychkovskyi, R.; Shavarskyi, I.; Saik, P.; Lozynskyi, V.; Falshtynskyi, V.; Cabana, E. Research into stress-strain state of the rock mass condition in the process of the operation of double-unit longwalls. *Min. Miner. Depos.* **2020**, *14*, 85–94. [CrossRef]
5. Yang, P.J.; Zhang, S.R.; Wang, X.F. Numerical Study on the Characteristics and Control Method of Coal Leakage between Supports in Integrated Mining of Extremely Loose and Soft Coal Seams. *Energies* **2024**, *17*, 1013. [CrossRef]
6. Zholmagambetov, N.; Khalikova, E.; Demin, V.; Balabas, A.; Abdrashev, R.; Suiintayeva, S. Ensuring a safe geomechanical state of the rock mass surrounding the mine workings in the Karaganda coal basin. *Min. Miner. Depos.* **2023**, *17*, 74–83. [CrossRef]
7. Xie, J.L.; Xu, J.L.; Wang, F. Mining-induced stress distribution of the working face in a kilometer-deep coal mine-a case study in Tangshan coal mine. *J. Geophys. Eng.* **2018**, *15*, 2060–2070. [CrossRef]
8. Zhang, Y.J. Distribution law of floor stress during mining of the upper protective coal seam. *Sci. Prog.* **2020**, *103*, 0036850420930982. [CrossRef] [PubMed]
9. Xiong, T.G.; Chang, J.C.; He, K.; Su, Y.F.; Qi, C. Study on deformation and failure characteristics of surrounding rock of overlying roadway under upward mining in the deep mine. *Geofluids* **2021**, *2021*, 5667183. [CrossRef]
10. Shan, R.L.; Wei, Y.H.; Wang, C.H.; Li, Z.; Zhao, Y.; Tong, X.; Xiao, S. Research on the evolution of the deviatoric stress and control of a gas extraction roadway under mining influence. *Environ. Earth Sci.* **2023**, *82*, 425. [CrossRef]
11. Guo, X.F.; Li, Y.G.; Zhou, G.D.; He, Z.; Yu, H.; Xu, Y. Stability analysis and reasonable layout of floor drainage roadway above confined water and under mining influence. *Geofluids* **2021**, *2021*, 5578717. [CrossRef]
12. Li, Y.E.; Ma, N.J.; Ma, J.; Zhang, H.; Gao, Z. Characteristics of perimeter rock damage and reasonable location of deep pressurized water upper bottom pumping tunnel. *J. Coal* **2018**, *43*, 2491–2500.
13. Li, A.; Ma, Q.; Lian, Y.Q.; Ma, L.; Mu, Q.; Chen, J. Numerical simulation and experimental study on floor failure mechanism of typical working face in thick coal seam in Chenghe mining area of Weibei, China. *Environ. Earth Sci.* **2020**, *79*, 118. [CrossRef]
14. Lu, C.J.; Xu, J.P.; Zhao, H.; Zhang, H.; Zhang, Y.; Chen, M. Floor disturbance and failure characteristics of super-large mining height working face. *Geofluids* **2022**, *2022*, 1279642. [CrossRef]
15. Zhang, D.M.; Sun, G.Y.; Li, G. Stability analysis and maintenance program design of roadway in remining coal seams under the influence of double mining. *J. Eng. Geol.* **2021**, *29*, 1028–1036.
16. Xiao, T.Q.; Bai, J.B.; Xu, L.; Zhang, X. Characteristics of stress distribution in floor strata and control of roadway stability under coal pillars. *Min. Sci. Technol.* **2011**, *21*, 243–247. [CrossRef]
17. Tang, Y.S.; Sun, W.C.; Zhang, X.; Liu, P. Effect of Advancing Direction of Working Face on Mining Stress Distribution in Deep Coal Mine. *Adv. Civ. Eng.* **2021**, *2021*, 7402164. [CrossRef]
18. Yu, Y.; Zhang, L.Y.; Lu, J.F.; Chen, D.; Zhao, X.; Liu, L. Research on the evolution characteristics of floor stress and reasonable layout of roadways in deep coal mining. *Geofluids* **2021**, *2021*, 6631444. [CrossRef]
19. Wang, Z.Q.; Wu, C.; Shi, L.; Su, Z.H.; Wang, P.; Huang, X. Analysis of surrounding rock stress and plastic zone of two-way unequal pressure circular roadway based on complex variable theory. *J. Coal* **2019**, *44*, 419–429.
20. Peng, Y.J.; Li, Q.F. Floor failure and roadway deformation induced by contiguous coal seams mining at Huopu Mine. *Arab. J. Geosci.* **2020**, *13*, 601. [CrossRef]
21. Cui, J.F.; Wang, W.J.; Jia, Q.; Peng, G.; Wu, H. Measurement and analysis of roadway deformation and stress under mining-induced stress. *Shock. Vib.* **2021**, *2021*, 5561093. [CrossRef]
22. Zhu, Y.; Yang, K.; Li, Y.L.; Li, W. Stability analysis and control countermeasures of laminated bottom plate in mining roadway under different coal pillar sizes. *J. Min. Saf. Eng.* **2023**, *40*, 467–479.
23. Gao, S.; Yang, J.; Gao, D.; Ouyang, Y.B.; Chai, J. Lay-out pattern and deformation law of mining roadway incontiguous coal seam mining. *J. Xi'an Univ. Sci. Technol.* **2022**, *42*, 191–199.
24. Chi, X.L.; Yang, K.; Fu, Q.; Dou, L. The mechanism of mining-induced stress evolution and ground pressure control at irregular working faces in inclined seams. *Geotech. Geol. Eng.* **2020**, *38*, 91–107. [CrossRef]
25. Dinmohammadpour, M.; Nikkhah, M.; Goshtasbi, K.; Ahangari, K. Application of the Kaiser Effect in In-situ Stress Measurement in Rocks-an overview. *Rud.-Geol.-Naft. Zb.* **2022**, *37*, 1–6. [CrossRef]
26. Sun, Y.X. Research on the deformation mechanism of mining roadway stratiform surrounding rock with nonuniform stress field. *Shock. Vib.* **2021**, *2021*, 6624045. [CrossRef]
27. Nehrii, S.; Nehrii, T.; Zolotarova, O.; Volkov, S. Investigation of the geomechanical state of soft adjoining rocks under protective constructions. *Rud.-Geol.-Naft. Zb.* **2021**, *36*, 14–22. [CrossRef]
28. Wang, P.; Jiang, L.S.; Ma, C.Q.; Yuan, A. Evolution Laws of Floor Stress and Stability of Floor Roadway Affected by Overhead Mining. *Earth Sci. Res. J.* **2020**, *24*, 45–54. [CrossRef]
29. Zhang, D.; Bai, J.B.; Yan, S.; Wang, R.; Meng, N.; Wang, G. Investigation on the failure mechanism of weak floors in deep and high-stress roadway and the corresponding control technology. *Minerals* **2021**, *11*, 1408. [CrossRef]

30. Tian, M.L.; Han, L.J.; Yang, X.X.; Feng, Q.; Meng, Q.; Xie, Y.; Li, W.; Ma, C. Asymmetric deformation failure mechanism and support technology of roadways under non-uniform pressure from a mining disturbance. *Bull. Eng. Geol. Environ.* **2022**, *81*, 211. [CrossRef]
31. State Administration of Work Safety; State Administration of Coal Mine Safety. *Regulation on Prevention and Control of Coal and Gas Outburst*; Coal Industry Press: Beijing, China, 2009.
32. Wang, Z.Q.; Yan, E.; Lu, G.D.; Gao, L.T.; Zhang, Q.M.; Tang, R.X. Statistical analysis of the distribution pattern of ground stress field in the reservoir site area of groundwater sealed hole reservoirs in mainland China. *Geotechnics* **2014**, *35*, 251–256.
33. Cao, W.X.; Liu, H.L.; Hang, Y.G.; Wang, H.; Li, G. Similarity simulation on the movement characteristics of surrounding rock and floor stress distribution for large-dip coal seam. *Sensors* **2022**, *22*, 2761. [CrossRef] [PubMed]
34. Song, Z.Q.; Wen, Z.J.; Jiang, Y.J.; Jiang, J.Q.; Shi, Y.K. Key theories and engineering applications of mining dynamics and rock control. *J. Coal* **2023**, 1–21. [CrossRef]